Topology optimization of geothermal bore fields using the method of moving asymptotes

A new method is proposed to optimize the configurations of vertical ground heat exchangers using topology optimization and the method of moving asymptotes. The problem formulation minimizes the required number of boreholes of a given length with simultaneous constraints on the entering fluid temperature in cooling and heating mode. The method relies on the adaptation of the alternative ASHRAE design method and a new analytical formulation for the calculation of g-functions based on a boundary condition of equal average fluid temperature. The method is applied to large bore fields consisting of more than a hundred boreholes. The paper also studies the effect of different types of domains and ground load profiles on the optimized configurations. It is shown that the shape of the domain has minimal impact on the optimized configurations. A higher density of boreholes on the perimeter of the domain compared to the center is recommended in the case where one operation mode is dominant. A uniform configuration is better suited when the load profile is balanced.

Keywords: Geothermal energy, ground heat exchangers, topology optimization, method of moving asymptotes, g-functions.

Introduction

The design of ground heat exchangers (GHE) is an important part of its installation as it directly affects the performance of the system, its safe operation and its cost. The design process also has to deal with constraints such as the available area, the ground properties and the technical limits for building the GHE. It is often necessary to have multiple boreholes given all these constraints, which together form a bore field. However, the performance of the individual boreholes decreases, as there is thermal interaction between the boreholes. The placement of the boreholes then becomes a challenge, as the cost and the total drilling length can increase drastically, which are two major obstacles in the adoption of the technology on a large scale.

Current state of GHE design

Traditionally, bore field designs are obtained by calculating the required drilling length for a predetermined configuration. The designer can then modify the placement of the boreholes as well as their number to improve the design. ASHRAE's sizing method is often used for this purpose. It is a three-pulse method, which describes a family of methods for which the bore field is sized according to three successive loads (Ahmadfard and Bernier 2019). The following equation governs ASHRAE's sizing method as reformulated by Bernier (2006):

$$L_{tot} = \frac{q_a R_{ga} + q_m R_{gm} + q_h R_{gh} + q_h R_b^*}{(T_m - T_g)_{ref} - \Delta T_p} \quad (1)$$

where L_{tot} is the total drilling length, q_a, q_m and q_h are the mean annual ground load, the mean monthly ground load for the design month and the hourly peak ground load for the design month, R_{ga}, R_{gm} and R_{gh} are the ground thermal resistances associated with each of the ground loads, R_b^* is the effective borehole thermal resistance, T_m is the mean fluid temperature circulating in the boreholes, T_g is the undisturbed ground temperature and ΔT_p is the temperature penalty. The temperature difference between the fluid and the ground is imposed in Equation (1). The simplest approach is to place the boreholes in a regular configuration in the given domain (e.g. on a rectangular grid) and modify the number of boreholes and the spacing until satisfying results are obtained.

Determining the value of ΔT_p is a challenge when using this method and its definition differs depending on how the ground thermal resistances are calculated. The ASHRAE Handbook (ASHRAE 2019) presents ΔT_p as a way to account for the thermal interactions between the boreholes. Other definitions of the temperature penalty include the one proposed by Fossa (2011) who evaluates the temperature penalty value of a

given bore field based on the fact that most ground thermal models are equivalent for short time periods. The temperature penalty ΔT_p can therefore be expressed as a correcting factor between an approximate model and the true value of the temperature drop or increase at the borehole wall for long time periods. Ahmadfard and Bernier (2018) modified Equation (1) by calculating the ground thermal resistances using g-functions:

$$L_{tot} = \frac{q_a R_{ga} + q_m R_{gm} + q_h R_{gh} + q_h R_b^*}{(T_m - T_g)_{ref}} \quad (2)$$

Using g-functions removes the necessity of the temperature penalty since they already consider thermal effects that arise over long time periods, namely thermal interactions between boreholes and axial effects. Since these effects are included in the ground thermal model used to evaluate the thermal resistances, there is no need for the temperature penalty and $\Delta T_p = 0$.

The research on bore field configurations has shown the importance of the placement of boreholes on the total drilling length as well as on the temperature distribution. Cimmino and Bernier (2014a) studied the effect of adding and removing boreholes by reducing and increasing the spacing in a regular configuration. They evaluated the required drilling length for the different cases by calculating the fluid temperature exiting the boreholes. They concluded that removing boreholes by increasing the spacing between them usually leads to an increase in the individual drilling length of the boreholes, but that the total drilling length is reduced. Bore fields should have the least possible amount of boreholes covering the available surface to improve the drilling length, as long as economical and technical constraints are still respected. Guo et al. (2017) proposed another analysis of the placement of boreholes on a given domain. They progressively displaced the boreholes located in the center of the

bore field towards the perimeter starting from a conventional design to optimize the variation of the ground temperature over the operation time of the bore field. They showed that the configurations that present a higher density of boreholes on the perimeter lead to more uniform temperature distribution in the ground. Spitler, Cook, and Liu (2020) studied various design strategies and their impact on the total drilling length and the temperature of the fluid entering the heat pump. This analysis proposed to investigate configurations with different regular spacing, irregularly spaced configurations (increased spacing in the center compared to the perimeter) and wrap-around configurations (boreholes are positioned around the building). It showed that these various strategies lead to savings in drilling length and thus reinforced the idea that irregular bore field configurations could improve the design of GHEs.

When strictly considering the minimal drilling length, two concepts stand out from these empirical investigations. The first one is that it is usually better to reduce the number of boreholes to fulfil the energy demand by making them as long as possible. The second one is that the density of boreholes should be higher on the perimeter of the bore field than in its center. The different strategies presented have shown promising results, which are usually better than more traditional design methods. The research has now shifted toward the optimization of bore field configurations by developing automated design methods.

Beck et al. (2013) proposed a method to optimize both the positions and the thermal loads of the individual boreholes using differential evolution to minimize the maximum temperature variation of the ground due to the bore field operation. The boreholes were located toward the perimeter of the bore field when optimizing the positions. They also concluded that there were limited benefits to optimize both the positions and the loads. Bayer, de Paly, and Beck (2014) developed a procedure to

optimize the thermal load of each borehole while also reducing the number of required boreholes. Starting from a regularly spaced configuration, the method relies on identifying the boreholes located where the temperature in the ground varies the most and removing them from the configuration. The objective function is once again the maximum ground temperature variation. The optimized configurations present the same characteristics as what was previously presented: the boreholes that were removed were located in the center, leaving only the ones on the perimeter. They however noted that removing too many boreholes could lead to a greater increase in the maximum temperature variation. Egidi, Giacomini, and Maponi (2023) optimized borehole positions using the steepest descent method, which required a derivable formulation of the heat transfer in the ground. The optimization problem minimizes the overall temperature variation in the ground for a given number of boreholes, where the available domain is not fixed. The results showed that the optimized configurations make use of as much space as possible (increased spacing between the boreholes). GHEDT (Cook 2021) and its updated version GHEDesigner (Spitler, West, and Liu 2022), are automated tools for the design of ground heat exchangers. The designer is able to choose between various placement routines depending on the design needs. Its newly implemented RowWise method gives the ability to place the boreholes irregularly while keeping an organized structure in different areas of the domain.

Topology optimization

Topology optimization originated in mechanical design to find the placement of material that will give the best structural performance (Sigmund and Maute 2013). The solutions to these types of problem are discrete on every area of the domain (i.e. material or no material). Topology optimization has evolved greatly over time and found applications in other fields of studies. This paper will only cover the concepts of

topology optimization that are relevant to the present GHE problem and the proposed method.

Many topology optimization methods are density based. For any given domain, the area is discretized and a density variable ($\boldsymbol{\rho}$) is introduced, which takes the value of 0 or 1 on every element and represents the design variable. Topology optimization problems are often non-convex and present non-unique solutions. The discretization of the domain introduces many discrete optimization variables (ρ_i), making the use of global optimization methods computationally expensive or unfeasible. One way to solve the problem is to make the design variable continuous so that efficient gradient-based optimization algorithms can be used, while still forcing the convergence to discrete solutions. This is the purpose of the Solid Isotropic Material with Penalization (SIMP) (Bendsøe 1989) method. The idea behind this method is to introduce a penalization term ($p \geq 1$) in the problem formulation, which penalizes intermediate values of the design variable and thus helps the convergence to values of 0 or 1. When $p > 1$, the problem becomes non-convex and has multiple local minima. The continuation approach is introduced to help the convergence toward the global minimum by solving the problem multiple times starting from a penalization of $p = 1$, and by slowly increasing its value using an increment (Δp) with the last solution as the new initial point for the next solving step. It should however be mentioned that the continuation approach does not guarantee the convergence to the global optimum even though it still represents a good approximation of its value (Svanberg and Stolpe 2001; Watada and Ohsaki 2009).

An example of an optimization algorithm used in topology optimization is the Method of Moving Asymptotes (MMA) (Svanberg 1987, 2002). The purpose of this method is to optimize nonlinear problems that are constrained by inequality functions. The MMA is a sequential optimization algorithm that constructs a convex

approximation of the constrained non-linear optimization problem (called subproblem in MMA terminology) based on the latest information on the objective function, the constraint functions, and the derivatives of the objective and constraint functions. The approximation is convex and separable, which allows computationally-efficient solutions to the subproblem, even for large numbers of optimization variables and multiple constraints. The MMA is globally convergent, meaning it should find an optimum given any starting point for the optimization.

Bore field configurations have proven to be an important part of the design process. Research has shown that irregular bore field configurations have the potential to reduce the number of boreholes required and thus reduce the initial cost of investment. It has motivated the development of sizing methods that work on the optimization of the placement of boreholes to reduce the total drilling length. Because of its nature, topology optimization and the SIMP method could represent a new approach to the design of GHEs. This paper proposes a method to design GHEs that minimizes the required number of boreholes by strategically placing them using the principles of topology optimization. The method includes constraints on both the minimum and maximum entering fluid temperatures in heating and cooling modes, respectively. It is an extension of the method proposed by Noël & Cimmino (2022). The additions include a temperature penalty in the definition of the constraints of the problem to account for the differences between different boundary conditions in the evaluation of the g-functions, as well as a new strategy to refine the domain based on the distribution of the design variable.

Methodology

The objective of the proposed bore field optimization method is to minimize the number of boreholes required given a specific domain and ground loads, where the individual

length of the boreholes is predetermined. The geometry of the boreholes and the thermal parameters that are considered are summarized in Figure 1, where L represents the length of the boreholes, D is the buried depth of the boreholes, r_b is the radius of the boreholes, and T_g, α_s, and k_s are respectively the undisturbed ground temperature, the thermal diffusivity of the soil and the thermal conductivity of the soil.

The optimization is constrained by the maximum allowable variation of the average fluid temperature circulating in the boreholes, both in heating and cooling modes. The alternative ASHRAE sizing method is adapted so that it is compatible with the SIMP method and the MMA. The superposition of the finite line source (FLS) is used to evaluate approximate g-functions and evaluate ground thermal resistances considering the design variable. This approximate formulation allows the analytical evaluation of derivatives of the constraint functions required for the MMA. The temperature penalty is then evaluated using a more accurate g-function formulation. A soft constraint on the minimal spacing between two consecutive boreholes is introduced by penalizing the thermal interaction between two possible borehole positions when they are closer than an imposed minimal spacing.

The following sections describe the methodology starting by the problem formulation, followed by the optimization procedure and then the handling of the grid throughout the optimization.

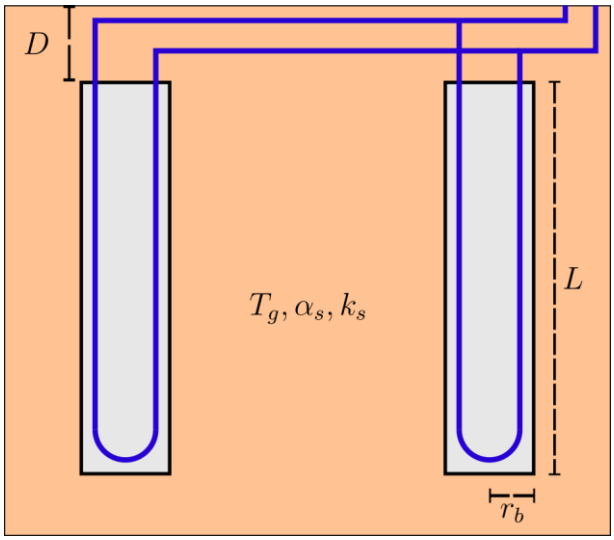

Fig. 1. Borehole geometry and thermal parameters

Problem formulation

The domain is discretized into nodes that each represent a possible borehole position. The method then finds the combination of boreholes of length L located at some of the possible positions that minimizes the total number of boreholes. The MMA requires the evaluation of the derivatives of the cost-function and the constraint functions. It is thus preferable that the functions used to formulate the problem are derivable to avoid increased computational costs for the numerical evaluation of derivatives. Two models for the evaluation of the g-function used with the alternative ASHRAE method will be developed using different boundary conditions. The first model is an approximation of the g-function based on the superposition of the finite line source solution. This model is used in the optimization procedure since it allows for the evaluation of analytical derivatives of the cost and constraint functions. The second model imposes a boundary condition of uniform fluid temperature along the length of the boreholes for the evaluation of the g-function. This model is then used to evaluate the temperature penalty but its impact on the derivatives is neglected.

The optimization problem is formulated as follows:

$$\begin{cases} Minimize: f_0(\boldsymbol{\rho}) = \sum_{i=1}^{n} \rho_i \\ Subject\ to: f_1(\boldsymbol{\rho}) = \left(T_m - T_g\right)_c - \left(T_m - T_g\right)_{ref,c} \leq 0 \\ f_2(\boldsymbol{\rho}) = \left(T_g - T_m\right)_h - \left(T_g - T_m\right)_{ref,h} \leq 0 \\ 0 \leq \rho_i \leq 1 \; for \; i = 1, \ldots, n \end{cases} \tag{3}$$

where $\boldsymbol{\rho} = [\rho_1 \quad \cdots \quad \rho_n]^T$ is the vector of borehole presence fractions ρ_i on any given node i inside the discretized domain, f_0 is the objective function, f_1 is the constraint in cooling, f_2 is the constraint in heating, and $(T_m - T_g)_{\text{ref,c}}$ and $(T_g - T_m)_{\text{ref,h}}$ are the maximum temperature differences between the ground and the fluid circulating inside the boreholes in cooling and in heating modes, respectively (i.e. the temperature constraints).

A value $\rho_i = 0$ signifies the absence of a borehole at node i of the domain, whereas a value $\rho_j = 1$ signifies the presence of a borehole at node j. In the context of the MMA, the presence of a borehole is taken as a continuous variable with values $0 \leq \rho_i \leq 1$. Non-integer values of the borehole presence fraction are allowed during the optimization process but are expected to converge to 0 or 1 using the continuation approach.

Ground thermal model

The values of $\left(T_m - T_g\right)_c$ and $\left(T_g - T_m\right)_h$ are evaluated using the alternative ASHRAE sizing equation from imposed design hourly, monthly and annual loads in both heating and cooling modes. Its formulation is adapted to consider the design variable ($\boldsymbol{\rho}$). The temperature difference is evaluated as follows:

$$\left(T_m - T_g\right)_c = \frac{q_{a,c}R_{ga} + q_{m,c}R_{gm} + q_{h,c}R_{gh} + q_{h,c}R_b^*}{L \cdot \sum_{i=1}^{n} \rho_i} + \Delta T_{p,c} \tag{4}$$

$$\left(T_g - T_m\right)_h = -\left(\frac{q_{a,h}R_{ga} + q_{m,h}R_{gm} + q_{h,h}R_{gh} + q_{h,h}R_b^*}{L \cdot \sum_{i=1}^{n} \rho_i} + \Delta T_{p,h}\right) \tag{5}$$

with:

$$R_{ga} = \frac{g_0(t_f) - g_0(t_f - t_1)}{2\pi k_s} \quad (6)$$

$$R_{gm} = \frac{g_0(t_f - t_1) - g_0(t_f - t_2)}{2\pi k_s} \quad (7)$$

$$R_{gh} = \frac{g_0(t_f - t_2)}{2\pi k_s} \quad (8)$$

where $\Delta T_{p,c}$ and $\Delta T_{p,h}$ are the temperature penalties in cooling and heating mode, and $g_0(t_i)$ are approximations of the g-functions evaluated at t_f, t_f - t_1 and t_f - t_2, with t_1 = 10 years, $t_2 = t_1$ + 1 month and $t_f = t_2$ + 6 hours as recommended in the alternative ASHRAE sizing method.

The approximations of the g-functions are evaluated using the superposition of the finite line source (FLS) solution as proposed by Claesson and Javed (2011):

$$g_0(t) = \frac{\boldsymbol{\rho}^T [b_{ij} h_{ij}] \boldsymbol{\rho}}{\sum_{i=1}^{n} \rho_i^p} \quad (9)$$

with:

$$h_{ij} = \frac{1}{2L} \int_{1/\sqrt{4\alpha_s t}}^{\infty} \frac{1}{s^2} \exp\left(-d_{ij}^2 s^2\right) I_{ls}(Ls, Ds) ds \quad (10)$$

$$I_{ls}(Ls, Ds) = 2 \cdot ierf(Ls) + 2 \cdot ierf(Ls + 2Ds) - ierf(2Ls + 2Ds) - ierf(2Ds) \quad (11)$$

where h_{ij} is the thermal response factor of a borehole positioned on the j-th node to a borehole positioned on the i-th node, p is a penalization for the SIMP method and will be explained later, and b_{ij} is a positive factor that acts as a soft constraint to ensure a minimal spacing (B_{min}) between two consecutive boreholes, d_{ij} is the radial distance

between the i-th and the j-th node (with $d_{ii} = r_b$, the borehole radius). If $d_{ij} < B_{min}$, $b_{ij} = 5$, otherwise it is equal to 1. The value of 5 is arbitrary, but it has been found to provide the desired effect. Note that Equation (9) allows for intermediate values of the design variable $\boldsymbol{\rho}$ (i.e. $0 < \rho_i < 1$). When all values are equal to 0 or 1, and using $p = 1$ and $b_{ij} = 1$, Equation (9) becomes equivalent to the method of Claesson and Javed (2011).

Derivatives of the cost- and constraint functions

The derivatives of the cost-function and the constraint functions are needed to apply the MMA. The derivative of the objective function f_0 in Equation (3) is given by:

$$\frac{\partial(f_0)}{\partial \boldsymbol{\rho}} = [1, \dots, 1]^T \tag{12}$$

and the derivatives of the constraint functions are given by:

$$\frac{\partial(f_1)}{\partial \boldsymbol{\rho}} = \frac{q_{a,c}\frac{\partial R_{ga}}{\partial \boldsymbol{\rho}} + q_{m,c}\frac{\partial R_{gm}}{\partial \boldsymbol{\rho}} + q_{h,c}\frac{\partial R_{gh}}{\partial \boldsymbol{\rho}}}{L\sum_{i=1}^{n}\rho_i} - \frac{q_{a,c}R_{ga} + q_{m,c}R_{gm} + q_{h,c}R_{gh} + q_{h,c}R_b^*}{L\left(\sum_{i=1}^{n}\rho_i\right)^2} \tag{13}$$

$$\frac{\partial(f_2)}{\partial \boldsymbol{\rho}} = -\left(\frac{q_{a,h}\frac{\partial R_{ga}}{\partial \boldsymbol{\rho}} + q_{m,h}\frac{\partial R_{gm}}{\partial \boldsymbol{\rho}} + q_{h,h}\frac{\partial R_{gh}}{\partial \boldsymbol{\rho}}}{L\sum_{i=1}^{n}\rho_i} - \frac{q_{a,h}R_{ga} + q_{m,h}R_{gm} + q_{h,h}R_{gh} + q_hR_b^*}{L\left(\sum_{i=1}^{n}\rho_i\right)^2}\right) \tag{14}$$

The derivatives of the g-functions are required to evaluate the derivatives of the ground thermal resistance:

$$\frac{\partial R_{ga}}{\partial \boldsymbol{\rho}} = \frac{\frac{\partial g_0}{\partial \boldsymbol{\rho}}(t_f) - \frac{\partial g_0}{\partial \boldsymbol{\rho}}(t_f - t_1)}{2\pi k_s} \tag{15}$$

$$\frac{\partial R_{gm}}{\partial \boldsymbol{\rho}} = \frac{\frac{\partial g_0}{\partial \boldsymbol{\rho}}(t_f - t_1) - \frac{\partial g_0}{\partial \boldsymbol{\rho}}(t_f - t_2)}{2\pi k_s} \tag{16}$$

$$\frac{\partial R_{gh}}{\partial \boldsymbol{\rho}} = \frac{\frac{\partial g_0}{\partial \boldsymbol{\rho}}(t_f - t_2)}{2\pi k_s} \tag{17}$$

$$\frac{\partial g_0}{\partial \boldsymbol{\rho}} = \frac{1}{\sum_{i=1}^{n} \rho_i^p}\left(-p\boldsymbol{\rho}^{p-1} g_0 + (\boldsymbol{b} \circ \boldsymbol{h})\boldsymbol{\rho} + \boldsymbol{\rho}^T(\boldsymbol{b} \circ \boldsymbol{h})\right) \tag{18}$$

Temperature penalty

The assumption of a uniform heat transfer rate (UHTR) is made for the approximation of g-functions, instead of a uniform borehole wall temperature (UBWT) (Cimmino and Bernier 2014b) or an equal inlet fluid temperature (EIFT) (Cimmino 2015, 2019) which would both provide more accurate evaluation of g-functions. The UHTR condition is used for the estimation because derivatives of the g-functions are required for the method of moving asymptotes. These derivatives are difficult to evaluate for the other boundary conditions since their evaluation relies on the solution of a system of linear equations. A boundary condition of uniform average fluid temperature (UAFT) in the boreholes is used for the evaluation of g-functions, rather than any of the aforementioned UBWT and EIFT conditions. This boundary was introduced by Monzó et al. (2018) using the finite element method for the evaluation of g-functions. This method has been shown to provide similar accuracy to the EIFT boundary condition. It is adapted here to use the analytical finite line source solution. This new formulation provides the advantage of using the same thermal parameter R_b^* as in the temperature constraint functions (Equations (4)-(5)). It also allows using intermediate values of the borehole presence fraction.

The temperature penalty is evaluated as follows:

$$\Delta T_{p,c} = \frac{q_{a,c}\Delta R_{ga} + q_{m,c}\Delta R_{gm} + q_{h,c}\Delta R_{gh}}{L \cdot \sum_{i=1}^{n} \rho_i} \tag{19}$$

$$\Delta T_{p,h} = \frac{q_{a,h}\Delta R_{ga} + q_{m,h}\Delta R_{gm} + q_{h,h}\Delta R_{gh}}{L \cdot \sum_{i=1}^{n} \rho_i} \quad (20)$$

where the values of ΔR_{gi} are evaluated similarly as the thermal resistances from Equations (6)-(8) except that the g-functions are replaced by g-function variations as follows:

$$\Delta g(t) = g_1(t) - g_0(t) \quad (21)$$

where g_1 is the reference g-function.

The evaluation of the reference g-functions consists in the solution to a system of three sets of equations: (1) the spatial superposition of the finite line source solution, (2) a relation for the heat transfer rate at the borehole wall, and (3) a global energy balance. The n boreholes are discretized into n_s segments, with L_u the length of the u-th segment of a borehole.

The superposition of the finite line source solution yields a set of $n_s \cdot n$ equations:

$$T_g - T_{b,i,u} = \sum_{j=1}^{n} \sum_{v=1}^{n_s} \frac{h_{ij,uv}(t) q_{j,v}(t)}{2\pi k_s} \quad (22)$$

where $h_{ij,uv}$ is the thermal response factors of the v-th segment of a borehole positioned on the j-th node to the u-th segment of a borehole positioned on the i-th node, $q_{j,v}$ is the heat extraction rate per unit borehole length of the v-th segment of a borehole positioned on the j-th node, and $T_{b,i,u}$ is the borehole wall temperature of the u-th segment of a borehole positioned on the i-th node. No temporal superposition is considered so as to accelerate the method in the optimization process.

The fluid flowing through the boreholes is assumed to have the same temperature, uniform along the length of the boreholes. The effective thermal resistances of the boreholes are modulated using the borehole presence fraction:

$$q_{i,u}(t) = \frac{T_{b,i,u}(t) - T_f(t)}{R_b^*/\rho_i} \tag{23}$$

where T_f is the uniform fluid temperature. The modulation of the effective thermal resistance makes it so that a value ρ_i = 0 yields an infinite thermal resistance and no heat extraction, thereby effectively removing the borehole from the bore field.

The global energy balance is given by:

$$\bar{q}(t) = \frac{\sum_{j=1}^{n}\sum_{v=1}^{n_s} L_{j,v} q_{j,v}(t)}{L \cdot \sum_{i=1}^{n} \rho_i} = \frac{\sum_{j=1}^{n}\sum_{v=1}^{n_s} L_{j,v} q_{j,v}(t)}{L_{tot}} \tag{24}$$

where $\bar{q}$ is the average heat extraction rate per unit borehole length in the bore field.

The system of Equations (22)-(24) is solved in non-dimensional form assuming a constant average heat transfer rate per unit borehole length. The dimensionless parameters are: $\Theta_{b,i,u} = \frac{T_g - T_{b,i,u}}{\bar{q}/2\pi k_s}$ the dimensionless borehole wall temperature, $\Theta_f = \frac{T_g - T_f}{\bar{q}/2\pi k_s}$ the dimensionless fluid temperature, and $\tilde{q}_{i,u} = q_{i,u}/\bar{q}$ the normalized heat extraction rate per unit borehole length. The system of equations becomes:

$$\sum_{j=1}^{n}\sum_{v=1}^{n_s} h_{ij,uv}(t)\tilde{q}_{j,v}(t) = \Theta_{b,i,u} \tag{25}$$

$$\sum_{i=1}^{n}\sum_{u=1}^{n_s} L_{i,u}\, \tilde{q}_{i,u}(t) = L_{tot} \tag{26}$$

$$\frac{2\pi k_s R_b^*}{\rho_i}\tilde{q}_{i,u}(t) + \Theta_{b,i,u} = \Theta_f \tag{27}$$

The g-function is then given by the effective dimensionless borehole wall temperature, as defined by Cimmino (2019):

$$g_1(t) = \Theta_f - 2\pi k_s R_b^* \quad (28)$$

Optimization procedure

The following section details the specific aspects of the proposed optimization procedure, which are summarized in Figure 2. The procedure starts with the solution of the optimization problem using the MMA with p = 1 and $\Delta T_{p,c}$ = $\Delta T_{p,h}$ = 0 on a uniform grid. The resulting distribution of the borehole presence fraction is then used to generate progressively refined non-uniform grids at subsequent solutions of the optimization problem. The subsequent solutions involve successive solutions of the optimization problem with increasing values of penalization, p. The temperature penalties, $\Delta T_{p,c}$ and $\Delta T_{p,h}$, are updated at the same time the penalization is increased.

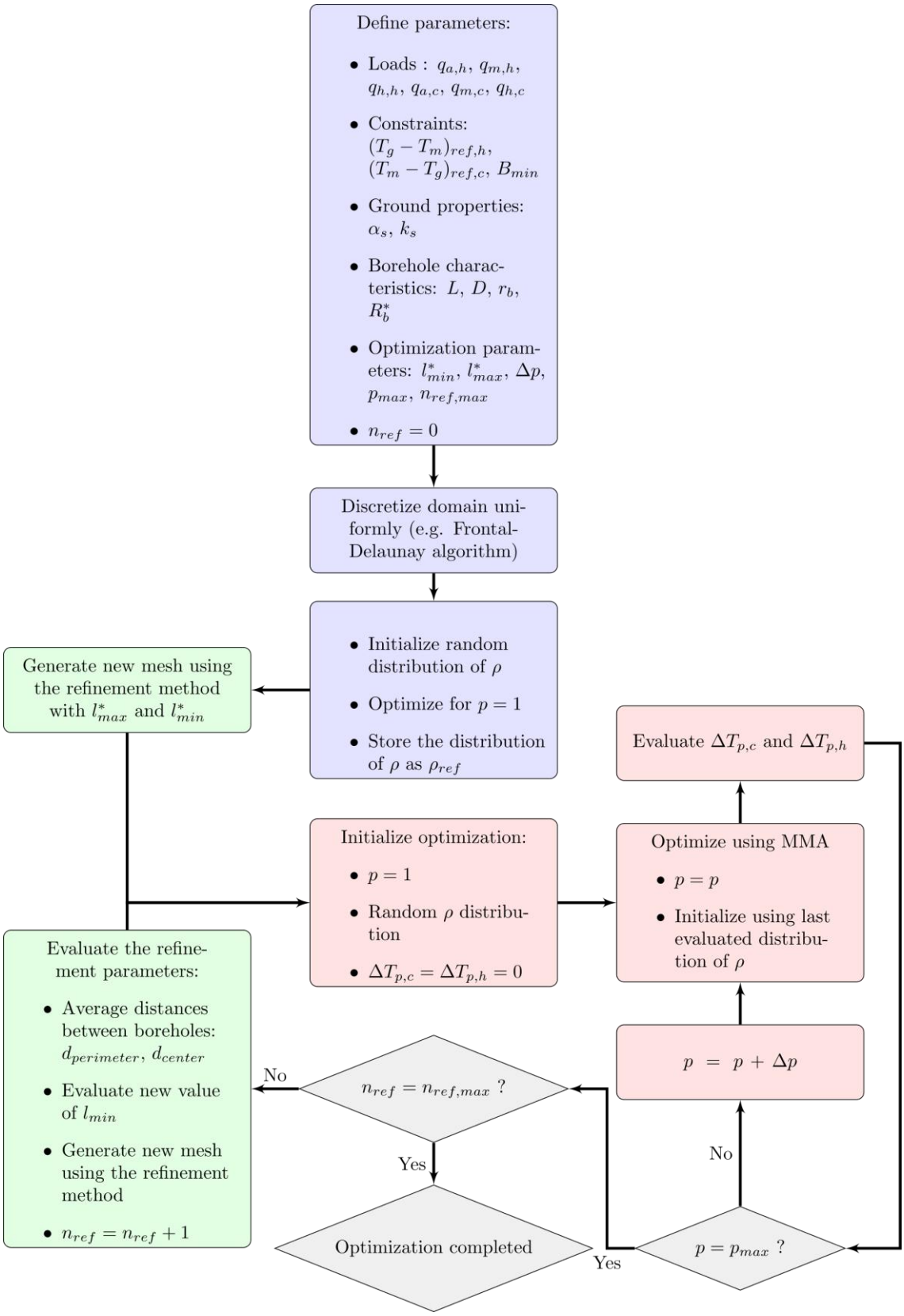

Fig. 2. Bore field optimization procedure

Penalization

The SIMP method consists in solving the optimization problem multiple times, where the penalization is increased in small increments, Δp, starting from p = 1. This procedure is known as the continuation approach. Typically, the increments are fixed throughout the procedure although adaptive penalization schemes have been proposed, e.g. Tarek and Ray (2020). The choice of the penalization step is crucial to avoid converging too quickly towards a local minimum. A constant step Δp = 0.01 and a maximum penalization p_{max} = 3 are used in the proposed method. The choice of p_{max} = 3 as the maximum penalization value comes from the uses of the SIMP method in structural design, where this limit is commonly used. In the case of the GHE problem, this penalization range led to the desired effect without any modification.

Temperature penalty

The values of $\Delta T_{p,c}$ and $\Delta T_{p,h}$ are assumed to be independent of $\boldsymbol{\rho}$ during the solution of the optimization problem (Equation (3)). Their values are only updated when the penalization is incremented, using the optimized borehole presence fraction from the latest optimization to evaluate the g-function g_1 with the UAFT boundary condition.

The accuracy of the g-function evaluation depends on the discretization of boreholes into segments, where using more segments leads to better accuracy. However, a higher number of segments results in a larger system of equations to solve and an increase in computation time. Here, even though the g-function only has to be solved at three time steps, it has to be solved each time the penalization is increased. A non-uniform discretization is adopted, as proposed by Cimmino and Cook (2022). The authors recommend 8 segments per borehole. Using 8 segments with the proposed optimization method is still expensive in computational time because of the domain

discretization. Solving the system of equations using 5 non-uniform segments per borehole was found to be a good compromise between accuracy and computational time, as the gains in minimizing the cost-function are less important for more segments.

Grid refinement

The level of discretization of the grid is an important aspect to consider in the optimization of the bore field. Using more nodes, which translates to more possible positions for the boreholes, typically improves the results of the optimization. It is however costly in terms of computation time to increase the number of nodes inside the grid. The grid should ideally be more refined in the areas where the boreholes are more likely to be located since the location of the boreholes has a greater impact on the thermal interaction in those regions. It is proposed to optimize the problem in three steps to obtain such a grid. A first optimization without penalization (i.e. $p = 1$) is performed on a uniform grid. A second optimization with penalization is done on a grid with finer discretization where a higher density of boreholes is located, using the first optimization to infer the expected distribution of boreholes. The third optimization with penalization is performed with a refined grid, using the first and second optimizations to infer the expected distribution of boreholes.

The first optimization (with $p = 1$) is conducted on a uniform grid with a characteristic length of 5m. This optimization yields a distribution of borehole presence fraction $\boldsymbol{\rho_{ref}}$ with intermediate values $0 \leq \rho_i \leq 1$. An example distribution is shown on Figure 3 for a square domain. While this distribution does not allow to position boreholes in the domain, it gives an indication of where boreholes are most likely to be optimally placed. On Figure 3, it can be seen that a higher density of boreholes, indicated by higher borehole presence fractions, is expected along the perimeter of the

domain. The distribution $\boldsymbol{\rho_{ref}}$ can thus be used to generate refined grids with higher density of nodes in these locations.

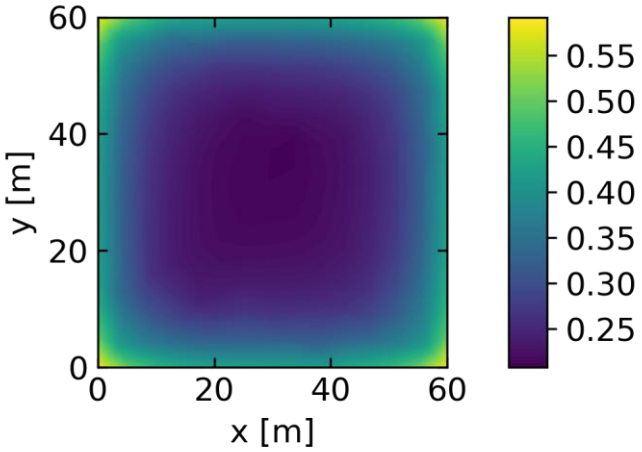

Fig. 3. ρ distribution for an optimized bore field with a penalization of $p = 1$

The distribution $\boldsymbol{\rho_{ref}}$ is then normalized between 0 and 1:

$$\widehat{\boldsymbol{\rho}} = \frac{\boldsymbol{\rho_{ref}} - \min(\boldsymbol{\rho_{ref}})\boldsymbol{J}}{\max(\boldsymbol{\rho_{ref}}) - \min(\boldsymbol{\rho_{ref}})} \tag{29}$$

where $\boldsymbol{J}$ is a vector of ones of the same dimension as the number of nodes on the reference grid. The value of $\widehat{\boldsymbol{\rho}}$ is then used in the subsequent stages of the refinement. The normalized distribution is scaled between l^*_{min} and l^*_{max}, the nominal minimum and maximum element sizes, so that the regions where the $\boldsymbol{\rho}$ distribution is higher will have a higher density of nodes:

$$\boldsymbol{l} = (\boldsymbol{J} - \widehat{\boldsymbol{\rho}})(l^*_{max} - l^*_{min}) + l^*_{min}\boldsymbol{J} \tag{30}$$

where $\boldsymbol{l}$ represents the refined element size of the new grid at all node locations $(\boldsymbol{x_{ref}}, \boldsymbol{y_{ref}})$ of the initial grid. The refined non-uniform grid is generated using a linear interpolation of $\boldsymbol{l}$ for the element sizes on the domain. The second optimization problem is solved with the continuation approach starting from p = 1 to p = 3.

For the third optimization, the domain is further refined using the last distribution of $\boldsymbol{\rho}$. The following parameters are calculated for the grid refinement:

$$d_{perimeter} = \frac{domain\ perimeter}{\sum \rho_{perimeter}} \tag{31}$$

$$d_{center} = \left(\frac{domain\ area}{\sum \rho_{center}}\right)^{0.5} \tag{32}$$

$$d_{min} = \min\left(d_{perimeter}, d_{center}\right) \tag{33}$$

$$d_{max} = \max\left(d_{perimeter}, d_{center}\right) \tag{34}$$

$$l_{min} = \frac{d_{min}}{d_{max}} l^*_{max} \tag{35}$$

where $d_{perimeter}$ and d_{center} are respectively a measure of the distance between full length boreholes on the perimeter and on the center of the grid, and$d$ l_{min} is the minimum element size of the third grid.

A new distribution of $\boldsymbol{l}$ is evaluated by replacing the value of l^*_{min} in Equation (30) with the newly calculated value of l_{min}, and a new refined grid is generated, once again by a linear interpolation. Figure 4 presents an example of the evolution of the grid for the three-step optimization technique.

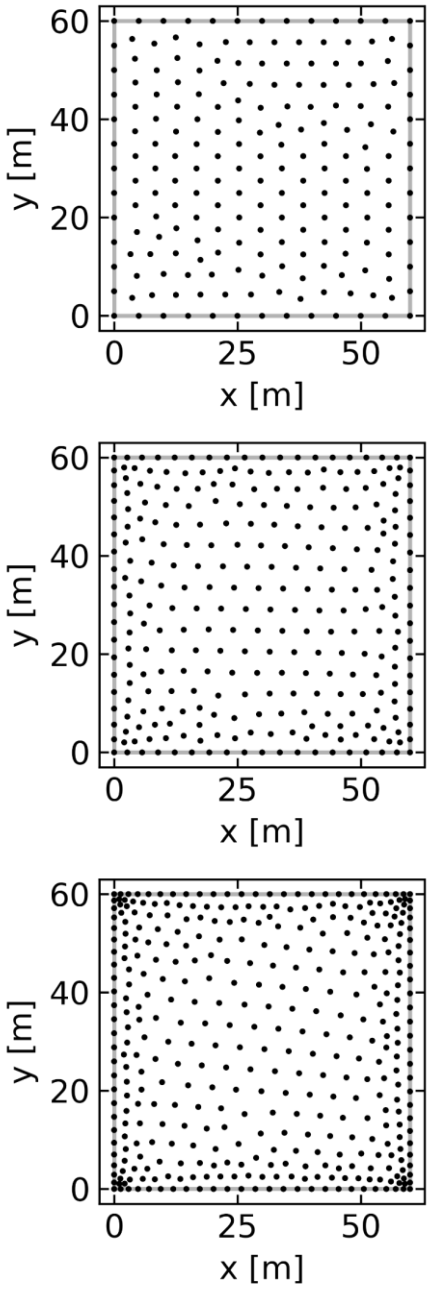

Fig. 4. Comparison between the initial grid (top), the initial function-defined grid (middle) and the refined function-defined grid (bottom)

In the case where $l_{min} \geq l_{min}^{*}$ in Equation (35), a third optimization is not necessary as repeating the optimization on a coarser grid will not improve the results. In this case, the procedure can be stopped and the results of the second optimization correspond to the optimized configuration. The refinement procedure used to generate

the third grid can be repeated more than once with updated values for l_{min}. The variable $n_{ref,max}$ can be defined as the maximum number of refinements to be performed before stopping the procedure.

Tools used in the implementation

The finite line source solution used to calculate g-functions is evaluated using *pygfunction* with the method of similarities (Cimmino 2018; Cimmino and Cook 2022). The *NLopt* 2.7.1 module (Johnson 2021) and its implementation of the MMA is used to solve the optimization problem. The generation and the refinement of the grid is performed using *pygmsh* 7.1.17 (Schlömer 2022), which is a Python interface for *Gmsh* (Geuzaine and Remacle 2009). *Gmsh* proposes a Frontal-Delaunay algorithm as default, based on the work of Rebay (1993). The Python module *trimesh* (Dawson-Haggerty 2022) is also used for processing the grid.

Results

The topology optimization method is applied to different load profiles on three different domains which all present similar area over perimeter ratios. The first domain is an L-shaped domain of 6800m^2 (Grid 1). The second domain is a circle with a radius of 38m (Grid 2) and finally the third domain is a square of 113m by 113m with an empty space of 20m by 40m where no boreholes can be placed (Grid 3). The effect of the temperature penalty is also explored. Finally, different load cases are presented as well as their effect on the optimized configurations. The objective of this study is to explore how different domain shapes and ground load profiles affect the optimal configuration of boreholes in a domain.

Table 1 presents the parameters used in the simulation concerning the bore field, the ground and the fluid circulating in the pipes. The parameters are similar to the ones

presented in Noël and Cimmino (2022). The major difference concerns the ground loads. The same annual ground loads are used, but the monthly and the hourly ground loads are scaled based on the annual load to produce different heat load profiles.

Table 1. Bore Field Parameters

Bore field parameters		
Borehole buried depth (D)	4	m
Borehole radius (r_b)	0.075	m
Borehole length (L)	125	m
Borehole thermal resistance (R_b^*)	0.2	m-K/W
Ground properties		
Thermal diffusivity (α_s)	1×10^{-6}	m^2/s
Thermal conductivity (k_s)	2.0	W/m-K
Undisturbed ground temperature (T_g)	14	°C
Annual ground load (q_a)	108.6	kW
Fluid properties (propylene-glycol 20% concentration)		
Flow rate ($\dot{V}_f$)	0.05	L/s-kW of peak load
Density ($\rho_{f,c}$)	1008	kg/m^3
Density ($\rho_{f,h}$)	1020	kg/m^3
Specific heat capacity ($c_{p,f,c}$)	4014	J/kg-K
Specific heat capacity ($c_{p,f,h}$)	3941	J/kg-K
Entering fluid temperature - heating mode ($T_{f,h}$)	0	°C
Entering fluid temperature - cooling mode ($T_{f,c}$)	40	°C

The constraints $\left(T_m - T_g\right)_{ref,c}$ and $\left(T_g - T_m\right)_{ref,h}$ are evaluated based on the fluid properties presented in Table 1 as follows:

$$T_{out,c} = T_{f,c} - \frac{1000}{\dot{V}_f \cdot \rho_{f,c} \cdot c_{p,f,c}} \tag{36}$$

$$T_{out,h} = \frac{1000}{\dot{V}_f \cdot \rho_{f,h} \cdot c_{p,f,h}} - T_{f,h} \tag{37}$$

$$T_{m,c} = \frac{T_{f,c} + T_{out,c}}{2} \tag{38}$$

$$T_{m,h} = \frac{T_{f,h} + T_{out,h}}{2} \tag{39}$$

where $T_{out,c}$ is the maximum outlet fluid temperature in cooling mode and $T_{out,h}$ is the minimum outlet fluid temperature in heating mode. For the given input parameters, the values of $T_{m,c}$ and $T_{m,h}$ are respectively 37.5°C and 2.5°C. Therefore, $\left(T_m - T_g\right)_{ref,c}$= 23.5°C for the constraint in cooling, and $\left(T_g - T_m\right)_{ref,h}$ = 11.5°C for the constraint in heating. Note that $\dot{V}_f$ has units of L/s-kW of peak load.

Table 2 presents four different parameter sets for the optimization. The first case serves as the base case and includes the temperature penalty. The second case uses the same ground loads as case 1 but the temperature penalty is assumed to be zero (i.e. only the approximation of the g-function is used for the optimization). For case 3, it is assumed that the hourly peak load is the same as the monthly load. Case 4 presents a balanced profile in heating and cooling. The value of q_a for this case is 0kW, and values for the hourly and the monthly load are based on the value of the annual load as presented in Table 1. The optimization parameters and variables are finally presented in Table 3. The constraint on the minimal spacing between to boreholes of 2.5m is smaller than what is typically found in current applications. The reason for using a spacing as

close as this is to find what the theoretical optimal configurations could be if we were able to achieve such configurations, i.e. to study how thermally optimal bore fields are configured before adding any feasibility constraints. The domains were refined, and the configurations were optimized until reaching the value of $n_{ref,max}$, no matter if $l_{min} \geq l^*_{min}$. The number of boreholes and the total drilling length for the optimized configurations are presented in Tables 4 and 5. As will be discussed, some of the values of ρ_i do not always converge to 0 or 1. Table 4 presents the results as rounded to the next integer. Table 5 shows the results of $L \cdot \sum_{i=1}^{n} \rho_i$ and $L \cdot n_b$ in parenthesis. Note that all the results that appear on the subsequent figures were filtered to only show the values of $\rho_i \geq 0.5$ to help with the clarity of the image. The results that appear in the tables are unfiltered, which explains why there are some instances where the number of boreholes on the figure does not correspond to the number of boreholes in Table 4.

Table 2. Summary of the Different Cases

	$q_{m,h}$	$q_{h,h}$	$q_{m,c}$	$q_{h,c}$	T_p
Case 1 (Base case)	-0.5 · q_a	-2.5 · q_a	2.5 · q_a	7 · q_a	Yes
Case 2 (Omitting ΔT_p)	-0.5 · q_a	-2.5 · q_a	2.5 · q_a	7 · q_a	No
Case 3 ($q_h = q_m$)	-0.5 · q_a	-0.5 · q_a	2.5 · q_a	2.5 · q_a	Yes
Case 4 (q_a = 0kW)	-2.5 · q_a	-7 · q_a	2.5 · q_a	7 · q_a	Yes

Table 3. Optimization parameters

Minimal spacing (B_{min})	2.5	m
Maximal distance between nodes (l^*_{max})	2.5	m
Initial minimal distance between nodes (l^*_{min})	1.25	m
Fixed penalization step (Δp)	0.01	-
Maximal penalization value (p_{max})	3	-
Maximal number of grid refinements ($n_{ref,max}$)	2	-

Table 4. Total number of boreholes for all cases

	Case 1 (Base case)	Case 2 (Omitting ΔT_p)	Case 3 ($q_h = q_m$)	Case 4 (q_a = 0kW)
Grid 1 (L)	149	154	71	188
Grid 2 (Circle)	205	245	98	189
Grid 3 (Square)	123	124	61	188

Table 5. Total drilling length in meters for all cases

	Case 1 (Base case)	Case 2 (Omitting ΔT_p)	Case 3 ($q_h = q_m$)	Case 4 (q_a = 0kW)
Grid 1 (L)	18 552	19 249	8 757	23 402
	(18 625)	(19 250)	(8 875)	(23 500)
Grid 2 (Circle)	25 625	30 623	12 249	23 611
	(25 625)	(30 625)	(12 250)	(23 625)
Grid 3 (Square)	15 265	15 467	7 595	23 409
	(15 375)	(15 500)	(7625)	(23 500)

Case 1: Base case

This case represents the complete method and serves as a reference for comparison purposes. The temperature penalty is considered to account for a more accurate evaluation of the average fluid temperature. The results are presented in Figure 5 for all three domains. On a visual standpoint, all three domains share a common characteristic: there is a separation between the borehole distribution on the perimeter and inside the domain. There is a slight difference between Grids 1 and 3, and Grid 2. Configurations obtained for Domains 1 and 3 present a higher density of boreholes on the outside border for which the spacing is close to the imposed minimum. The boreholes that are not on the border are then positioned in what seems a uniform arrangement with increased spacing compared to the perimeter. The second grid is however divided in three zones. The first one is close to the perimeter and a layer of closely spaced boreholes is present, the second zone is located toward the middle of the domain. An agglomeration of boreholes is present and the spacing is increased compared to the border of the domain. The final distinct zone is located between the perimeter and the middle of the domain, where no boreholes are present.

The results obtained on the circle grid (Grid 2) did not all respect the soft constraint of B_{min} = 2.5m. One pair of boreholes are at a distance of 2.49m. This increases the value of the g-function but the effect should be minimal when taking into account that it only affects one pair of boreholes out of 205 boreholes.

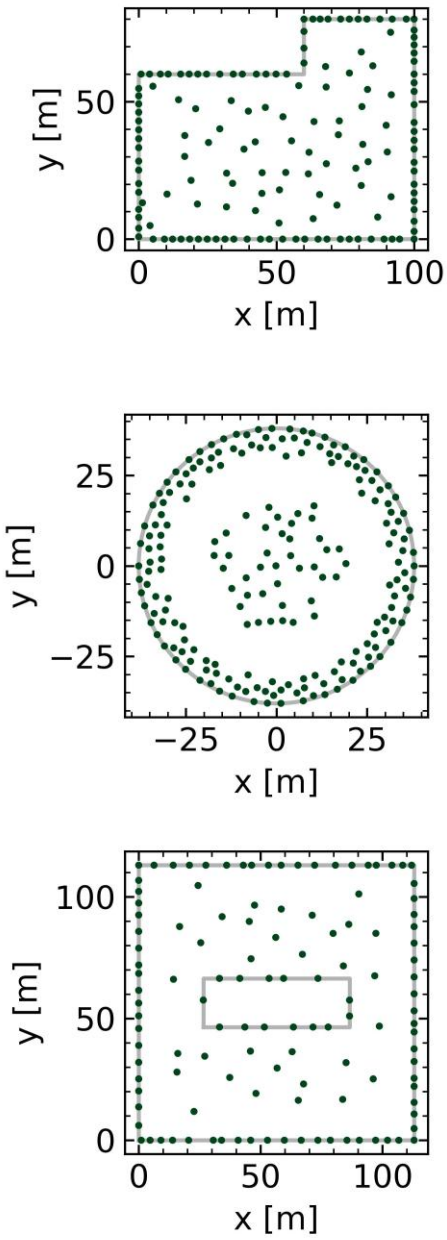

Fig. 5. Optimal configurations for case 1

Case 2: Omitting the temperature penalty

For case 2, the temperature penalty is not taken into consideration. This means that only the UHTR boundary condition is used in the evaluation of the g-functions. This case serves as a measure of the inaccuracy of the approximate method for the evaluation of g-functions. Results for case 2 are presented in Figure 6 for all three domains. The three

optimizations that were performed present the same visual appearance as case 1. However, it is shown that the inclusion of the temperature penalty has a non-negligible effect on the number of required boreholes inside the domain. The increase in the required number of boreholes is more important for Grid 2, for which the number of boreholes is significantly higher than the other two domains. This is expected due to the greater number of boreholes which increases thermal interactions and accentuates errors due to improper boundary conditions in the evaluation of g-functions (Cimmino and Bernier 2014b).

The same observation as case 1 can be made on the second grid where some of the boreholes do not respect the imposed minimal spacing. Five pairs of boreholes are closer than this value with the closest ones being 2.49m apart. The same conclusion can be made as to the effect of the non-respect of the constraint on the optimized configuration.

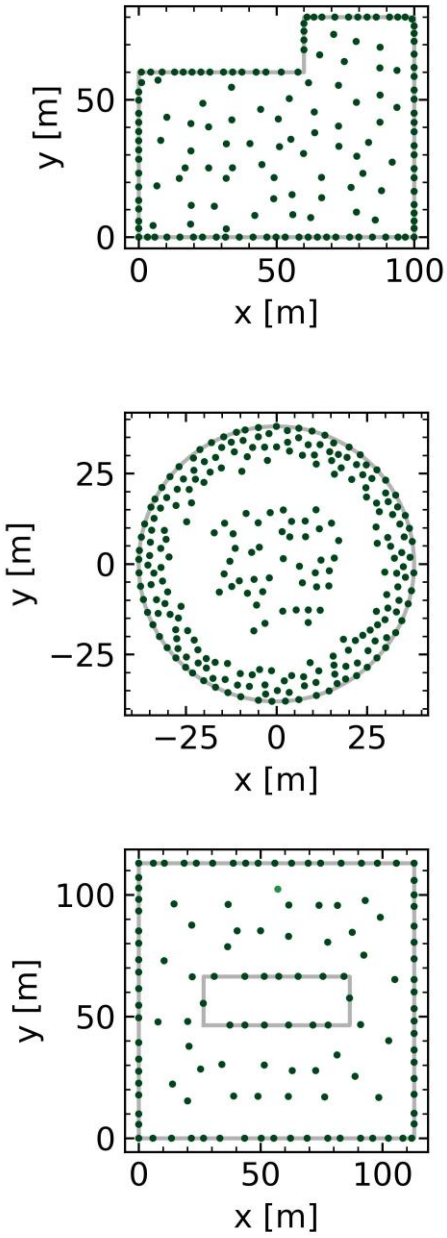

Fig. 6. Optimal configurations for case 2

Case 3: Equal hourly and monthly loads

For case 3, the hourly load is decreased compared to the first two cases. As a result, fewer boreholes are required to satisfy the heating and cooling energy demands. Results for case 3 are presented in Figure 7. The configuration of Grid 1 is very similar to what was presented in the first two cases. There is however one characteristic of this domain

that is more prominent. Since the shape is concave, there is a reflex angle on the upper part of the domain, and only one borehole is present close to this angle. Grid 2 presents a configuration with characteristics that are now more similar to what was obtained in the first two cases with Grids 1 and 3 in terms of density on the border and in the center of the bore field. Grid 3 respects the same principles highlighted previously concerning the density. However, since the number of boreholes is reduced, it is possible to observe that some of the boreholes on the perimeter are paired together, showing varying spacings on the perimeter.

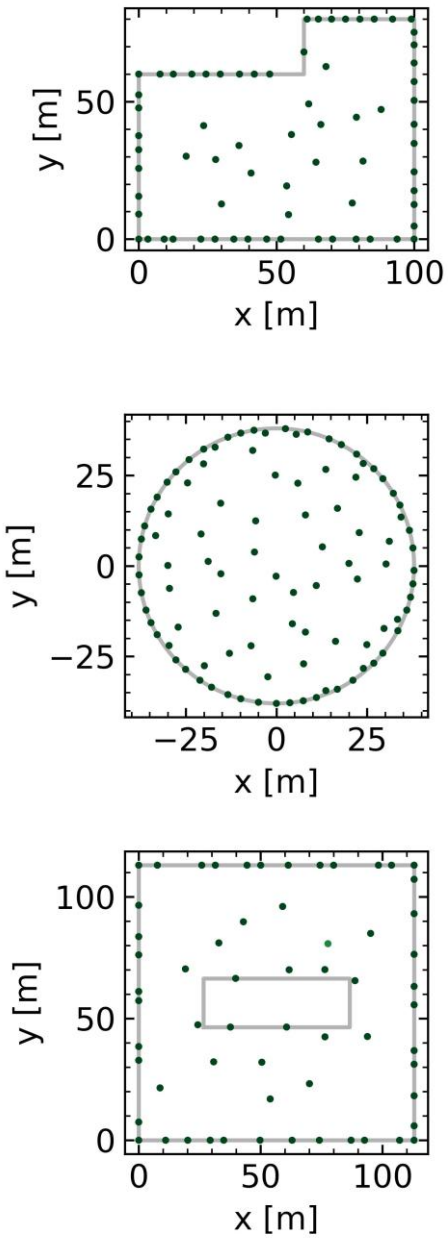

Fig. 7. Optimal configurations for case 3

Case 4: Balanced loads

The ground loads used for case 4 are perfectly balanced. The annual ground load is therefore equal to 0kW. The optimized configurations for case 4 are presented in Figure 8. The configurations obtained for this case are similar. The boreholes are positioned in every area of the domain and have an overall constant spacing. It is also

worth noting that even though the domains are different, the number of boreholes is the same. The values of $(T_m - T_g)_c$ and $(T_g - T_m)_h$ evaluated at the end of the optimization procedure are equal and the case is constrained in heating mode. This is different than the other cases where both values were different with the cooling mode being the more constraining of the two.

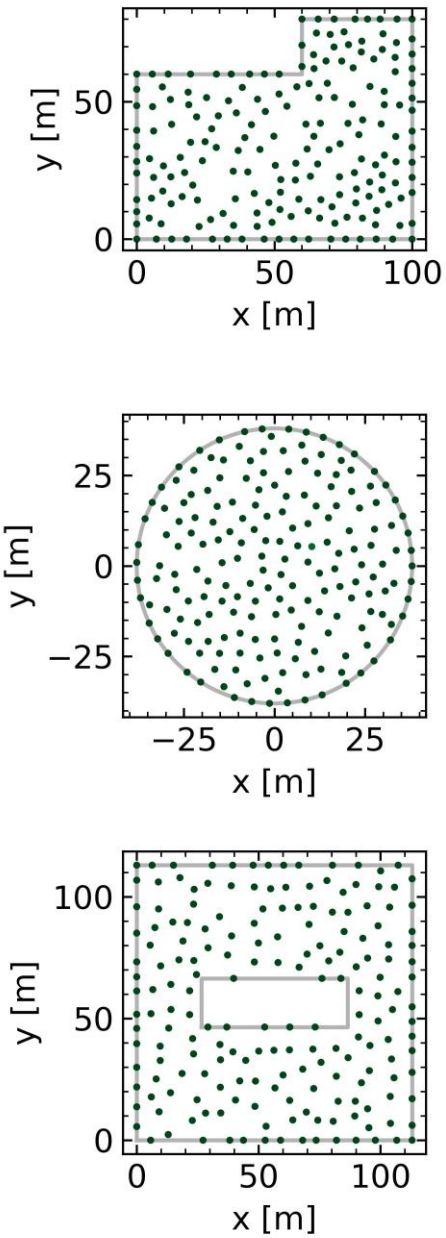

Fig. 8. Results for case 4

The optimization parameters were modified during this case for Grid 3, as the memory usage was too important for the available tools. The value of l^*_{max} was changed to 5m, and the value of l^*_{min} to 2.5m. This issue will be further discussed.

Discussion and conclusions

It is shown that the method is able to provide optimized bore field configurations. The method is an improved version of the optimization method presented by Noël & Cimmino (2022), with the addition of a temperature penalty to improve the accuracy of the thermal model, as well as a method to refine the discretized domain based on the distribution of the design variable on the first steps of the optimization process.

This paper has validated some of the research made on bore field optimization, showing that there is a gain in placing the boreholes irregularly. In most cases, placing the boreholes closer on the perimeter of the bore field and coarser towards the center leads to savings in drilling length.

Impact of ground load profile

Three load profiles were studied: a cooling dominant profile, a profile where the hourly peak and the monthly loads are equal with less heat injection and extraction, and a balanced profile.

In the case where one mode of operation is dominant, the optimized configurations converge to a higher density of boreholes on the perimeter than in the center as can be observed on cases 1 to 4. This characteristic was found in previous studies and is a way to limit the interactions between the boreholes. This is due to the overall ground temperature that will either increase or decrease depending on the dominant mode of operation. The results obtained on the circular domain show that another strategy is to regroup the boreholes located on the perimeter onto a layer of

closely spaced boreholes and to regroup the boreholes located in the center with a larger spacing than on the perimeter, leaving an empty zone between these two groups. These results only applied to cases 1 and 2 as the results for case 3 on the circular domain are similar to what was found on the other domains. This tends to suggest that the amount of heat to extract or to inject has a greater impact than the load profile itself, as long as one mode of operation is dominant. An increase in the heat transfer leads to more boreholes, and there seems to be a threshold for which the boreholes should be positioned in a manner that will leave part of the domain empty.

When the loads are smaller, and therefore the number of boreholes is reduced, a strategy was found on Grid 3 where the boreholes were positioned in pairs in some parts of the perimeter. This strategy seems to be only possible when the number of boreholes is small enough. It is interesting to note that this strategy was preferred compared to positioning more boreholes in the center or having an even spacing.

Finally, a balanced load profile generated configurations that were somewhat regular (constant spacing between all the boreholes on all parts of the domains). Since the annual load is 0kW, the soil does not tend to either warm or cool over a long period of time meaning that the interactions are limited when the boreholes are regularly spaced.

Impact of geometry

Conclusions may be made on concave geometries. The spacing between boreholes on Grid 1 was increased close to its reflex angle as opposed to the other parts of the perimeter. The effect was more pronounced when the overall heat injected and extracted was reduced in case 3. This showed that there is a benefit to varying the spacing on specific parts of the domain. A similar effect may be present on Grid 3 where the hole is positioned, but it is definitely harder to tell since the total number of boreholes is lower

on this grid. The effect on this grid could also be because the reflex angles are in the center of the domain, which, as was previously shown, usually has a lower density of boreholes.

Impact of the number of segments

The number of segments considered in the evaluation of the g-functions used to calculate the temperature penalty has an impact on both the computational costs and the precision of the results. A higher number of segments will lead to more precise results, but the drawback is that the size of the system of equations will greatly increase, especially in the case of the proposed method where a large number of points are generated in the grid.

The temperature penalty was evaluated for a varying number of segments to quantify the precision of the chosen 5 segments compared to the recommended 8 segments from Cimmino and Cook (2022). The optimized configuration for case 1 on Grid 1 is considered, and only the nodes where $\rho_i \geq 0.01$ are used. The results are presented in Table 6. The difference in the evaluation of the temperature penalty for 5 and 8 segments is 0.037°C. Table 6 also shows that using more than 5 segments leads to less improvement in precision every time the number of segments is increased, when compared to the improvements of increasing the number of segments up to 5. We can conclude that considering more than 5 segments has a minimal impact on the evaluation of the constraint, and that the increase in computational costs associated with the 8 segments is not justified for the purpose of the proposed method.

Table 6. Evaluation of the temperature penalty as a function of the number of segments on grid 1 for the case 1

	Cooling		Heating	
Number of segments	**ΔT_p (°C)**	**Difference with 8 segments (°C)**	**ΔT_p (°C)**	**Difference with 8 segments (°C)**
1	-0.044	0.548	0.036	0.547
2	-0.051	0.541	0.043	0.540
3	-0.403	0.189	0.394	0.189
4	-0.407	0.185	0.398	0.185
5	-0.556	0.037	0.546	0.037
6	-0.576	0.016	0.567	0.016
7	-0.588	0.004	0.579	0.004
8	-0.592	-	0.583	-

Limitations

The proposed grid refinement technique is able to refine the discretization in locations where there are more boreholes. However, the method is still heuristic in some aspects and some drawbacks of using this particular technique can be identified. Parameters are introduced to modulate the refinement and to limit the number of refinements that are performed. The parameter values used in this paper are not universal and may need adjustments if the methodology is applied to other cases.

The modulation based on the ratio d_{min}/d_{max} shown in equation (35) might refine the domain too much in cases where there is a great imbalance between d_{min} and d_{max}, even when the number of boreholes required is small. This can result in increased computation time and cost due to the generation of a grid with a large number of nodes,

as experienced on Grid 3 in case 4 where the optimization could not be performed using the same mesh refinement parameters as all the other optimizations.

The method still presents some of the limitations highlighted in Noël & Cimmino (2022). The configurations are too complex to be used as is by a designer. The optimized configurations should not be interpreted as an exact blueprint of where boreholes should be positioned but rather as a guide to identify what the spacing between boreholes should be in different areas of the domain. It is also worth reminding that the configurations likely converged to a local optimum, since the continuation approach of the SIMP method and the MMA do not guarantee the convergence to a global optimum. Using the continuation approach, the total number of boreholes and total drilling length should be close to the global optimum. The global optimal configuration of boreholes would differ as to the exact positions of the boreholes within the bore field. However, the thermal response of the bore field is not dependent on the exact positions of the boreholes but rather on the relative positions of the boreholes to one another (i.e. the density of boreholes in different areas of the domain). With this in mind, many configurations of boreholes will lead to similar thermal responses and therefore, total number of boreholes.

There are still occurrences of intermediate design variable values even though the SIMP method is applied to the optimization problem. There are instances where some of the nodes have converged to values of $\rho_i \leq 0.1$ but that are still greater than 0. These values can add up and increase the value of the sum of the design variable. In some other cases, an intermediate value of ρ_i closer to 1 can appear, meaning that the optimization has converged to an intermediate value of the design variable. A filtering followed by a re-evaluation of T_m might be necessary to eliminate these partial values while still ensuring that the constraints are respected.

The computational time of the method is mostly dependent on the number of nodes in the discretization of the domain. For the presented cases, the computational time for one refinement ranged from around 3 to 33.5 hours on grids ranging from 1333 to 3436 nodes. Note that the implementation of the method has not been optimized for computational performance at this stage.

Contributions

The presented method improves on preceding work on topology optimization of geothermal bore fields by Beck et al. (2013), Bayer, de Paly and Beck (2014), and Egidi, Giacomini and Maponi (2023) by directly minimizing the total number of boreholes and including simultaneous constraints on the minimum and maximum fluid temperatures in heating and cooling modes, respectively. The method is adapted from the well-established three-pulse ASHRAE sizing method and utilizes g-functions to accurately account for thermal interactions between boreholes and axial effects within the bore field. The method handles large bore fields with more than a hundred boreholes and thousands of possible borehole positions.

Load profiles and geometries were shown to play a role in the determination of the configurations. The strategies uncovered using the proposed topology optimization method were to position boreholes closer on the perimeter as opposed to the center in case of an imbalanced load profile, to limit the number of boreholes located near reflex angles, and to group boreholes in pairs on the perimeter when it is possible to do so. This shows that studying a wide range of load profiles and geometries can lead to various design strategies.

This work also presented an analytical solution to evaluate g-functions based on an equal average fluid temperature for all boreholes. This method for calculating

g-functions was used to improve the precision of the fluid temperature evaluation in the constraint functions of the optimization problem and adapted to include the design variable of the optimization problem. It showed that the inclusion of the newly added temperature penalty based on this analytical solution can leads to a lower evaluation of the total drilling length.

Future work

Future work will focus on the economic optimization of bore field configurations. The quantification of a feasibility indicator for bore field configuration, which could be used to drive the optimization process toward simpler design, will also be explored.

Nomenclature

$\boldsymbol{b}$ = Array of soft constraint on the minimal spacing between two nodes

b_{ij} = Soft constraint on the minimal spacing between two nodes

B_{min} = Constraint on the minimal spacing between two boreholes

$c_{p,f}$ = Fluid specific heat capacity

D = Borehole buried depth

$\boldsymbol{d}$ = Array of radial distance between two nodes

$d_{perimeter}$ = Measure of the distance between the boreholes on the perimeter of the domain

d_{center} = Measure of the distance between the boreholes in the center of the domain

d_{ij} = Radial distance between two nodes

d_{min} = Minimum value between $d_{perimeter}$ and d_{center}

d_{max} = Maximum value between $d_{perimeter}$ and d_{center}

EIFT = Equal Inlet Fluid Temperature

FLS = Finite Line Source

f_0 = Objective function

f_1 = Optimization constraint in cooling

f_2 = Optimization constraint in heating

Δg = g-function variation

g_0 = g-function approximation using uniform heat transfer rate condition

g_1 = Reference g-function

$\boldsymbol{h}$ = Array of thermal response factors between two nodes

h_{ij} = Thermal response factor between two nodes

$ierf$ = Error function integral

$\boldsymbol{J}$ = Vector of ones

k_s = Ground thermal conductivity

L = Borehole length

$\boldsymbol{l}$ = Element size distribution on the grid

l^*_{min} = Nominal minimum element size in the grid

l_{min} = Calculated minimum element size in the grid

l^*_{max} = Nominal maximum element size in the grid

L_{tot} = Total drilling length

MMA = Method of Moving Asymptotes

n = Design variable size

n_b = Number of boreholes

$n_{ref,max}$ = Maximum number of refinements

n_s = Number of borehole segments considered in the g-function evaluation

p = Penalization

Δp = Penalization step

q = Heat transfer rate

$\bar{q}$ = Average heat extraction rate per unit borehole length

$\tilde{q}$ = Normalized heat extraction rate per unit borehole length

q_a = Annual ground load

q_h = Hourly ground load

q_m = Monthly ground load

r_b = Borehole radius

R_b^* = Effective borehole thermal resistance

ΔR_{gi} = Ground thermal resistance variation

R_{ga} = Annual ground thermal resistance

R_{gh} = Hourly ground thermal resistance

R_{gm} = Monthly ground thermal resistance

SIMP = Solid Isotropic Material with Penalization

t = g-function time step

T_b = Borehole wall temperature

$T_{c,f}$ = Entering fluid temperature in cooling mode

T_f = Uniform fluid temperature

$T_{h,f}$ = Entering fluid temperature in heating mode

T_m = Average fluid temperature circulating in the boreholes

T_g = Undisturbed ground temperature

ΔT_p = Temperature penalty

UBWT= Uniform Borehole Wall Temperature

UHTR = Uniform Heat Transfer Rate

$\dot{V}_f$ = Fluid flow rate in the boreholes

$\boldsymbol{x_{ref}}$ = x coordinates of the nodes on the initial grid

$\boldsymbol{y_{ref}}$ = y coordinates of the nodes on the initial grid

Greek symbols

α_s = Ground thermal diffusivity

Θ_b = Dimensionless borehole wall temperature

Θ_f = Dimensionless fluid temperature

$\boldsymbol{\rho}$ = Design variable

ρ_{center} = Design variable for the nodes located in the center of the grid

ρ_f = Fluid density

$\rho_{perimeter}$ = Design variable for the nodes located on the perimeter of the grid

$\boldsymbol{\rho_{ref}}$ = Optimized design variable distribution on uniform grid without penalization

$\widehat{\boldsymbol{\rho}}$ = Normalized distribution of $\boldsymbol{\rho_{ref}}$

Acknowledgments

This work was supported by the Natural Sciences and Engineering Research Council of Canada [grant number RGPIN-2018-04471]. The authors acknowledge the Institut de l'Énergie Trottier and Hydro-Québec for a scholarship awarded to the first author.

Disclosure Statement

The authors report there are no competing interests to declare.

References

Ahmadfard, Mohammadamin, and Michel Bernier. 2018. "Modifications to ASHRAE's sizing method for vertical ground heat exchangers." *Science and Technology for*

the Built Environment 24 (7):803-817. https://doi.org/10.1080/23744731.2018.1423816.
———. 2019. "A review of vertical ground heat exchanger sizing tools including an inter-model comparison." *Renewable and Sustainable Energy Reviews* 110:247-265. https://doi.org/https://doi.org/10.1016/j.rser.2019.04.045.
ASHRAE. 2019. "35.1.3.1 Vertical Design." In *2019 ASHRAE® Handbook Heating, Ventilating, and Air-Conditioning Applications (I-P Edition)*, 35.31-35.51. Atlanta, GA: American Society of Heating, Refrigerating and Air-Conditioning Engineers, Inc. (ASHRAE).
Bayer, Peter, Michael de Paly, and Markus Beck. 2014. "Strategic optimization of borehole heat exchanger field for seasonal geothermal heating and cooling." *Applied Energy* 136:445-453. https://doi.org/https://doi.org/10.1016/j.apenergy.2014.09.029.
Beck, Markus, Peter Bayer, Michael de Paly, Jozsef Hecht-Méndez, and Andreas Zell. 2013. "Geometric arrangement and operation mode adjustment in low-enthalpy geothermal borehole fields for heating." *Energy* 49:434-443. https://doi.org/https://doi.org/10.1016/j.energy.2012.10.060.
Bendsøe, M. P. 1989. "Optimal shape design as a material distribution problem." *Structural Optimization* 1 (4):193-202. https://doi.org/10.1007/BF01650949.
Bernier, Michel. 2006. "Closed-Loop Ground-Coupled Heat Pump Systems." *ASHRAE Journal* 48 (9):12.
Cimmino, Massimo. 2015. "The Effects of Borehole Thermal Resistances and Fluid Flow Rate on the g-functions of Geothermal Bore Fields." *International Journal of Heat and Mass Transfer* 91:1119-1127. https://doi.org/https://doi.org/10.1016/j.ijheatmasstransfer.2015.08.041.
———. 2018. pygfunction: an opensource toolbox for the evaluation of thermal response factors for geothermal borehole fields. Paper presented at the eSim 2018, the 10th conference of IBPSA-Canada, Montréal, Canada, May 9-10.
———. 2019. "Semi-Analytical Method for g-Function Calculation of Bore Fields with Series- and Parallel-Connected Boreholes." *Science and Technology for the Built Environment* 25 (8):1007-1022. https://doi.org/https://doi.org/10.1080/23744731.2019.1622937.
Cimmino, Massimo, and Michel Bernier. 2014a. "Effects of Unequal Borehole Spacing on the Required Borehole Length." *ASHRAE Transactions* 120 (2):158-173.
———. 2014b. "A semi-analytical method to generate g-functions for geothermal bore fields." *International Journal of Heat and Mass Transfer* 70:641-650. https://doi.org/https://doi.org/10.1016/j.ijheatmasstransfer.2013.11.037.
Cimmino, Massimo, and Jonathan C. Cook. 2022. pygfunction 2.2: New Features and Improvements in Accuracy and Computational Efficiency. Paper presented at the International Ground Source Heat Pump Association Annual Conference, Las Vegas, Nevada, December 6-8.
Claesson, Johan, and Saqib Javed. 2011. "An analytical method to calculate borehole fluid temperatures for time-scales from minutes to decades." *ASHRAE Transactions* 117 (2):279-288.
Cook, Jonathan C. 2021. "Development of computer programs for fast computation of g-functions and automated ground heat exchanger design." M.S., Oklahoma State University.
Dawson-Haggerty, Michael. 2022. "trimesh." V. 3.11.2. https://trimsh.org/.
Egidi, Nadaniela, Josephin Giacomini, and Pierluigi Maponi. 2023. "Inverse heat conduction to model and optimise a geothermal field." *Journal of*

Computational and Applied Mathematics 423:114957. https://doi.org/https://doi.org/10.1016/j.cam.2022.114957.

Fossa, Marco. 2011. "The temperature penalty approach to the design of borehole heat exchangers for heat pump applications." *Energy and Buildings* 43 (6):1473-1479. https://doi.org/https://doi.org/10.1016/j.enbuild.2011.02.020.

Geuzaine, Christophe, and Jean-François Remacle. 2009. "Gmsh: A 3-D finite element mesh generator with built-in pre- and post-processing facilities." *International Journal for Numerical Methods in Engineering* 79 (11):1309-1331. https://doi.org/https://doi.org/10.1002/nme.2579.

Guo, Min, Nairen Diao, Ke Zhu, and Zhaohong Fang. 2017. "Optimization of Ground Heat Exchangers in Area with Imbalanced Heating and Cooling Load." *Procedia Engineering* 205:3727-3734. https://doi.org/https://doi.org/10.1016/j.proeng.2017.10.311.

Johnson, Steven G. 2021. "The NLopt nonlinear-optimization package." V. 2.7.1. http://github.com/stevengj/nlopt.

Monzo, Patricia, Anjan Rao Puttige, José Acuna, Palne Mogensen, Antonio Cazorla, Juan Rodriguez, Carla Montagud, and Fernando Cerdeira. 2018. "Numerical Modeling of Ground Thermal Response with Borehole Heat Exchangers Connected in Parallel." *Energy and Buildings* 172:371-394. https://doi.org/https://doi.org/10.1016/j.enbuild.2018.04.057.

Noël, Alexandre, and Massimo Cimmino. 2022. Development of a topology optimization method for the design of ground heat exchangers. Paper presented at the International Ground Source Heat Pump Association Annual Conference, Las Vegas, Nevada, December 6-8.

Rebay, S. 1993. "Efficient Unstructured Mesh Generation by Means of Delaunay Triangulation and Bowyer-Watson Algorithm." *Journal of Computational Physics* 106 (1):125-138. https://doi.org/https://doi.org/10.1006/jcph.1993.1097.

Schlömer, Nico. 2022. "pygmsh: A Python frontend for Gmsh." V. 7.1.17. https://github.com/nschloe/pygmsh.

Sigmund, Ole, and Kurt Maute. 2013. "Topology Optimization Approaches." *Structural and Multidisciplinary Optimization* 48:1031-1055. https://doi.org/https://doi.org/10.1007/s00158-013-0978-6.

Spitler, Jeffrey D., Jonathan C. Cook, and Xiaobing Liu. 2020. A Preliminary Investigation on the Cost Reduction Potential of Optimizing Bore Fields for Commercial Ground Source Heat Pump Systems. Paper presented at the 45th Workshop on Geothermal Reservoir Engineering, Stanford, California, February 10-12.

Spitler, Jeffrey D., Timothy West, and Xiaobing Liu. 2022. Ground Heat Exchanger Design Tool with RowWise Placement of Boreholes. Paper presented at the International Ground Source Heat Pump Association Annual Conference, Las Vegas, Nevada, December 6-8.

Svanberg, Krister. 1987. "The method of moving asymptotes—a new method for structural optimization." *International Journal for Numerical Methods in Engineering* 24 (2):359-373. https://doi.org/https://doi.org/10.1002/nme.1620240207.

———. 2002. "A Class of Globally Convergent Optimization Methods Based on Conservative Convex Separable Approximations." *SIAM journal on Optimization* 12 (2):555-573. https://doi.org/10.1137/S1052623499362822.

Svanberg, Krister, and Mathias Stolpe. 2001. "On the trajectories of penalization methods for topology optimization." *Structural and Multidisciplinary*

Optimization 21:128-139. https://doi.org/https://doi.org/10.1007/s001580050177.

Tarek, Mohamed, and Tapabrata Ray. 2020. "Adaptive continuation solid isotropic material with penalization for volume constrained compliance minimization." *Computer Methods in Applied Mechanics and Engineering* 363:1-22. https://doi.org/https://doi.org/10.1016/j.cma.2020.112880.

Watada, Ryo, and Makoto Ohsaki. 2009. "Continuation Approach for Investigation of Non-uniqueness of Optimal Topology for Minimum Compliance." In *8th World Congress on Structural and Multidisciplinary Optimization*, 1-10. Lisbon, Portugal.